JOURNAL OF MAGNETIC RESONANCE **135,** 61–69 (1998)
ARTICLE NO. MN981552

Multiple-Quantum MAS NMR Spectroscopy of Spin-$\frac{3}{2}$ Quadrupolar Spin Systems Using Shaped Pulses

Shangwu Ding and Charles A. McDowell[1]

Department of Chemistry, University of British Columbia, Vancouver, British Columbia, Canada V6T 1Z1

Received October 6, 1997; revised June 12, 1998

An investigation of the effect of shaping the pulses in multiple-quantum magic-angle nuclear magnetic resonance experiments was carried out on polycrystalline samples containing spin-$\frac{3}{2}$ quadrupolar nuclear spins. Both theoretical analysis and numerical simulations show that there exist types of shaped pulses that are more advantageous than the usual rectangular pulses in exciting multiple-quantum coherences and converting these into single-quantum coherences or zero-quantum coherences (in *z*-filtering cases). The sensitivities can be enhanced without loss of resolution or increasing the RF offset dependences. Moreover, properly shaped pulses can moderate the requirements on the RF power and sample spinning speeds. Especially important for application purposes is the finding that lattice site quantification can also be improved by the use of certain shaped pulses.

1. INTRODUCTION

The multiple-quantum magic-angle spinning (MQMAS) nuclear magnetic resonance (NMR) spectroscopic technique has engaged the attention of many scientists since Frydman and Hardwood (*1*) proposed the multiple-quantum coherence (MQC)–single quantum coherence (1QC) correlation technique to obtain the isotropic spectra of half-integer quadrupolar spin systems without using dynamic-angle spinning (DAS) (*2, 3*) or double-axis rotation (DOR) (*3, 4*) NMR techniques. Clearly, MQMAS is a significant enhancement of the repertoire of methods available for solid-state nuclear magnetic resonance studies. The two-pulse version of MQMAS which is experimentally simpler was subsequently found to produce higher sensitivities in addition to yielding better spectral lineshapes (pure absorptive) (*5–13*). Extensive studies involving numerical analysis and experimental verifications have been devoted to optimizing the pulse sequences for MQMAS NMR to achieve better sensitivities (*5–8, 12*). Although the techniques used to obtain pure absorptive lineshapes such as TPPI, and the hypercomplex method, have been applied in MQMAS studies, it has been the case that dispersion is frequently found to be still serious, especially for high coherences ($|p| > 3$) cases because of the asymmetry of the coherence transfers $0 \rightarrow \pm p$ for quadrupolar nuclear spin systems under RF pulse irradiation. This situation can be improved by application of the *z*-filtering method which ensures the symmetry of the intensities of the coherences before detection. The three-pulse version of the *z*-filtering method (*13*) is superior to its four-pulse counterpart (*14*) because the former yields higher spectral sensitivities and is more easily optimized. Further improvement of the spectral lineshapes can be achieved by synchronizing the sample spinning rate with the pulse lengths (*12, 15*). The presence of the spinning sidebands in the first dimension was detected and satisfactorily explained recently (*16, 17*).

Systematic comparisons between MQMAS NMR and VAS (variable-angle spinning), DAS, and DOR NMR techniques used in the study of quadrupolar nuclear spin systems have been published (*18, 19*). While the MQMAS method has rapidly become a favorite experimental choice, nevertheless, VAS, DAS, and DOR are complementary techniques for some systems and can be incorporated with MQMAS (*12, 19, 20*). A time-split method (*14, 21*) was proposed to avoid the shearing transformation of the spectral data which is usually needed as a post-data processing procedure to enhance the resolution in the first dimension of the 2D MQMAS NMR spectra. This renders data processing easier but the pure absorptivities of the resulting lineshapes are generally not as good as those obtained by the two-pulse-plus-*z*-filtering method (*13*). The incorporation of MQMAS with cross polarization (*22, 23*) and heteronuclear correlation (*24*) has been demonstrated to be useful in certain situations. Because of its experimental convenience, MQMAS has found many applications in studies of a large range of practical chemical systems of different complexities from simple inorganic compounds to catalysts and molecular sieves (*5, 18–37*). The high resolution achieved makes it easy to detect weak interactions involving quadrupolar spins, e.g., *J*-coupling between spin-$\frac{1}{2}$ and spin-$\frac{3}{2}$ nuclei (*38*).

Based on the results of the above investigations, MQMAS can at present be regarded as an important new "routine" experimental method in solid-state NMR. Site quantification of nuclei portrayed in the spectra acquired by the MQMAS NMR technique is, however, often found to be not wholly satisfactory, especially when the magnitudes of the quadrupolar cou-

[1] To whom correspondence should be addressed. Fax: (604) 822-2847. E-mail: mcdowell@chem.ubc.ca.

1090-7807/98 $25.00

pling constants (QCCs) of the nuclei at different crystal lattice sites in the system under investigation vary greatly. The common situation is that the intensities of the signals from lattice sites occupied by nuclei with large values of QCCs are reduced in magnitude. Recently, a method exploiting the nutation characteristics of the coherences of quadrupolar spins in rotating solids under RF irradiation, named RIACT (*39*) (*r*otation-*i*nduced *a*diabatic *c*oherence *t*ransfer), was proposed to yield better site quantitative MQMAS NMR spectra by carefully setting the pulse lengths according to the sample spinning speeds. Because the adiabatic condition for coherence transfer is better satisfied at higher spinning speeds for nuclei with larger QCCs (i.e., the difference between the effective quadrupolar frequencies is decreased by sample spinning), the intensities of the signals for sites occupied by nuclei with large values of QCCs can be relatively enhanced by using the RIACT method, hence yielding better site quantification of the MQMAS NMR spectra.

The goal of this paper is to present a method which holds promise for further improvement in site quantification by using properly shaped 3Q $\rightarrow$ 1Q (or 0Q) conversion pulses. In an earlier study (*40*), we reported that shaped 0Q $\rightarrow$ 3Q excitation pulses, which consume less RF power, may be used to enhance spectral sensitivity without losing resolution or reducing site quantification. In that work, however, only the first pulse (for MQC excitation) could be shaped because the conversion pulse was restricted to a duration of only a few microseconds. According to numerical simulations and experimental results, by the use of the RIACT pulse scheme (*39*), both the excitation and the conversion pulses used in MQMAS NMR employing that method can have lengths of tens, even hundreds, of microseconds, and, therefore, there are presented the possibilities for much more freedom to undertake extensive pulse shaping experiments. This can be understood because the second pulse is used primarily to convert the MQCs into 1QCs or 0QCs (in z-filtering cases magnetizations are stored along the z-axis of the laboratory frame as zero-quantum coherences and then transferred back to the observable single-quantum signal). In most quadrupolar spin systems, the MQCs spanning the $m \leftrightarrow -m$ transitions have rather narrow spectral widths which, therefore, can be excited uniformly when a long pulse is used. It is well known that whenever a long pulse is used, a properly shaped one often outperforms its rectangular counterpart in terms of excitation efficiency, homogeneity, tolerance to RF offset, and other experimental imperfections (*41*). In this work we presented both theoretical and experimental studies of spin-$\frac{3}{2}$ MQMAS NMR spectra obtained by using shaped pulses for the 3QC–1QC (0QC) conversion process. Advantageous pulse shapes are proposed and experimentally demonstrated to show that they offer better site quantitative MQMAS NMR spectra under less demanding experimental conditions than those frequently employed.

2. THEORY AND SIMULATION

The problem of obtaining the optimal conversion of certain orders of MQCs in quadrupolar systems can be generally expressed as follows: given the quadrupolar interaction Hamiltonian and initial density matrix, how can one optimize the RF Hamiltonian so that the greatest portion of the MQCs can be converted into 1QCs or 0QCs, in the z-filtering case (for uncoupled spin systems such as that studied in this work, it is to be noted that 0QCs correspond to the diagonal elements of the density matrix). In this work, spin-$\frac{3}{2}$ quadrupolar nuclear spin systems are investigated. The density matrix of the initial state of the system, $\rho(0)$, should be selected according to the case under study (see later). The total Hamiltonian can be expressed in the rotating frame as

$$H = \omega_q[I_z^2 - \tfrac{1}{3}I(I+1)] + \omega_1(t)I_\phi, \qquad [1]$$

where ω_1 is the amplitude of the RF field which is generally time dependent when shaped pulses are used. ϕ is the phase of the RF field. The quadrupolar frequency ω_q can be written as

$$\omega_q = \sqrt{6}\hbar \sum_{m,n=-2}^{+2} \mathcal{D}^{(2)}_{m0}(\omega_r t,\ \theta,\ 0)\mathcal{D}^{(2)}_{nm}(\alpha,\ \beta,\ \gamma)\rho^Q_{2n}. \qquad [2]$$

In this equation $\mathcal{D}$ is the Wigner rotational transformation matrix, and ρ^Q_{2n} represents the principal elements of the electric field gradient tensor. The Euler angles (α, β, γ) correspond to the transformation from the principal axis system (PAS) of the quadrupolar interaction tensor to the rotor axis frame. θ is the spinning axis direction relative to the direction of the applied magnetic field and ω_r is the rotor spinning rate.

The density matrix $\rho(t)$ at any time t (>0) is

$$\rho(t) = U(t,\ 0)^{-1}\rho(0)U(t,\ 0), \qquad [3]$$

where the evolution operator is written as

$$U(t,\ 0) = Te^{-i\int_0^t dt' H(t')}. \qquad [4]$$

Here T is the time-ordering operator. The ideal RF pulses in our case are those that provide the greatest sensitivity, give the best site quantitative spectra over a broad range of QCCs, have good offset tolerance, and do not present demanding experimental conditions such as very high sample spinning speeds. From the above equations, there is no physical reason that a rectangular pulse would be the best pulse shape to be employed in these experiments. In fact, we can regard the internal interaction H_Q during the pulsing period as an additional "pulse" which is spatially highly anisotropic and time depenent. The optimum value of the $\omega_1 I_\phi$ term should be chosen so that the effect of H_Q can be canceled (or utilized) and the maximum

3QC → 1QC (or 3QC → 0QC in the *z*-filtering case) conversion efficiency is achieved. Because usually Eq. [3] cannot be solved analytically, there are no general rules that can be used to identify the ideal pulse shapes. A straightforward theoretical analysis, however, is given here to show that the rectangular pulses normally used in MQMAS NMR studies are not necessarily the best in terms of optimal sensitivity, site quantification, RF offset tolerance, and requirements on spinning speed and other conditions. For this purpose an elementary application of Floquet theory (*42–46*) is employed. When rectangular pulses are used, since the RF term is time independent, the total Hamiltonian is periodical and, therefore, the evolution operator according to quantum Floquet theory can be written as

$$U(t_p) = P(t_p)e^{-iQt_p}P^{-1}(0), \qquad [5]$$

where $P(t)$ is periodical and Q is a time-independent traceless diagonal matrix (*42–46*). On the other hand, a pulse with arbitrary shape can be regarded as a cascade of very small rectangular pulses, each of which can be described by Eq. [5]; therefore, the total evolution operator for this case can be given as

$$U(t_p) = P(t_p)e^{-i\int_0^{t_p}Q(t')dt'}P^{-1}(0), \qquad [6]$$

where $P(t)$ is no longer necessarily periodical and Q may be time dependent. The signal after the conversion pulse(s) is determined by

$$S = \mathrm{Tr}[OU(t_p)\rho(0)U^{-1}(t_p)], \qquad [7]$$

where O is the observation (or detection) operator and $\rho(0)$ is the initial density matrix; both of these depend on the pulse scheme employed. For the normal two-pulse scheme employed in MQMAS NMR for quadrupolar spin-$\frac{3}{2}$ nuclei, $\rho(0)$ can be chosen as $I^{(14)} = |1\rangle\langle 4|$, and O as $I_x^{(23)}$. On the other hand the first pulse of the *z*-filtering scheme, $\rho(0)$, should be chosen as $|1\rangle\langle 4|e^{-i\omega_{14}t_1} + \mathrm{HC}$, where HC is the Hermitian conjugate. t_1 must be nonzero otherwise the populations $\rho_{22}(t_p)$ and $\rho_{33}(t_p)$ are equal (also see below). The detection operator is $I_z^{(23)}$. For the second pulse in the *z*-filtering case, $\rho(0) = I_z^{(23)}$ and O is $I_x^{(23)}$. It is not difficult, therefore, to verify that a properly shaped pulse is better than a rectangular pulse. For example, when the two-pulse scheme is used, the 1QC signal after the conversion pulse can be calculated from Eq. [5] as

$$\langle I_x^{(23)}\rangle = \sum_{l,m=1}^{4} P_{3l}(t_p)P_{m2}^{-1}(t_p)P_{4m}(0)P_{l1}^{-1}(0)e^{-i(Q_{ll}-Q_{mm})t_p} \qquad [8]$$

for a rectangular pulse, and

$$\langle I_x^{(23)}\rangle = \sum_{l,m=1}^{4} P_{3l}(t_p)P_{m2}^{-1}(t_p)P_{4m}(0)P_{l1}^{-1}(0)e^{-i\int_0^{t_p}(Q_{ll}(t')-Q_{mm}(t'))dt'} \qquad [9]$$

for a shaped pulse. Obviously, there are more adjustable parameters in Eq. [9] than in Eq. [8]. By a judicious choice of values of the parameters the signal thus can be better optimized. This point can be supported by numerical simulations. We will not go further into the details of the analysis based on Eqs. [8] and [9] in this work; these will be presented later. Instead, we will focus on demonstrating the characteristics of a number of shaped pulses, based on the above considerations, that are advantageous over the rectangular pulses normally used in MQMAS NMR experiments.

Following the earlier work on shaped pulses (*40*), other pulse shapes have been studied. For instance, when the conversion pulse takes the shape defined by

$$\omega_1(t) = a \sin b(t - t_0)/(t - t_0), \qquad [10]$$

where a, b, and t_0 are adjustable parameters, more site quantitative MQMAS NMR spectra can be obtained. On the other hand, the decaying exponential pulse, $\omega_{1\max}e^{-bt}$, has better RF offset tolerance (see later). The Fourier transform of Eq. [10] is a rectangle with a length of b; therefore, it represents uniform "excitation" over a range of b centered at zero frequency (actually the carrier frequency in the laboratory frame). Consequently, it can convert MQCs into 1QCs more uniformly, which means that better site quantitative MQMAS NMR spectra should result. Actually, as shown below, it can offer more than better site quantification. To demonstrate the advantages of employing shaped pulses in MQMAS experiments, a series of spectral simulations based on Eq. [3] was performed to compare the sensitivity, quantification, and offset tolerance for different pulse shapes.

The coherence conversion pulse was studied for two typical cases; e.g., the two-pulse scheme and a *z*-filtering scheme. As pointed out above, for the first case, the initial density matrix is chosen as

$$\rho(0) = I^{14} = |1\rangle\langle 4| \qquad [11]$$

which is the 3QC operator for spin-$\frac{3}{2}$ nuclear spin systems. The conversion efficiency can be calculated with the absolute value of the density matrix element $\rho_{1/2,-1/2}$.

In the *z*-filtering case, there are two pulses, so the initial density matrices differ. Because the population difference between $|\frac{1}{2}\rangle$ and $-|\frac{1}{2}\rangle$ is involved in the *z*-filtering case, care should be taken when choosing the initial density matrix. For instance, the seemingly reasonable choice of Eq. [11] is not

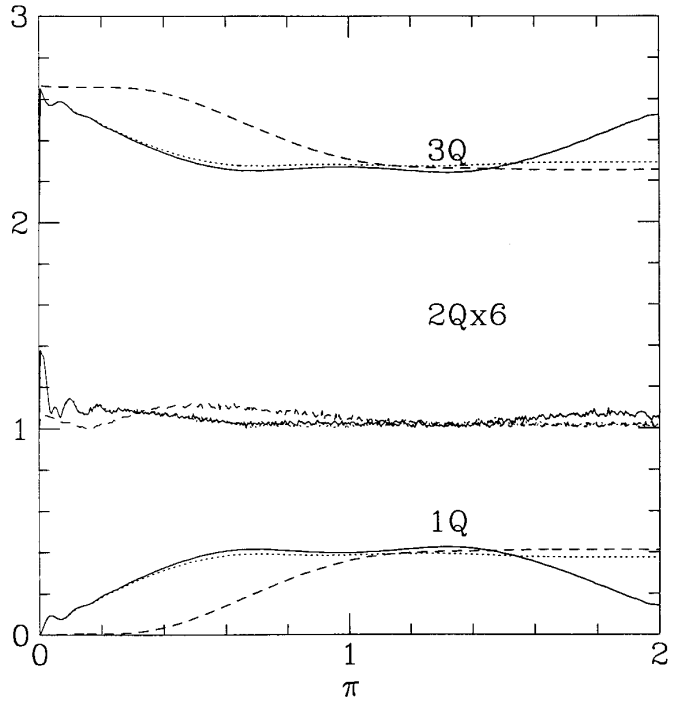

FIG. 1. The conversion efficiencies from the initial 3QC for different shaped pulses over a spinning period $[0,2\pi]$. The lines for the 2QC and 3QC cases were shifted vertically by 1 and 2 units, respectively. The dashed lines are for a rectangular pulse, the dotted lines for a decaying triangular pulse, and the solid lines for the pulse defined by Eq. [10]. The parameters used are Zeeman frequency $\omega_0 = 50.0$ MHz, quadrupolar coupling constant $e^2qQ/h = 2.4$ MHz with asymmetry parameter $\eta_Q = 0.8$, and the *moderate* sample spinning speed $\omega_r = 5.0$ kHz. For the rectangular pulse, the RF power is $\omega_1 = 60.0$ kHz for a decaying triangular pulse, the maximum RF power is $\omega_{max} = 60.0$ kHz for the pulse defined by Eq. [10], $a = 10\omega_1 = 600.0$ kHz, $b = 0.1\omega_1 = 6.0$ kHz, and $t_0 = 50.0$ μs.

suitable because the population difference would be zero regardless of the pulse shape. In fact, from the structure of the Hamiltonian (Eq. [1]), it is not difficult to show that the difference of the matrix elements $\rho_{1/2,1/2} - \rho_{-1/2,-1/2}$ is zero whenever the initial 3QC is in the x or y directions of the fictitious spin-$\frac{1}{2}$ space. Thus, the following general initial density matrix

$$\rho(0) = I^{14}(t_1) = |1\rangle\langle 4|e^{i\omega_{14}t_1} + |4\rangle\langle 1|e^{-i\omega_{14}t_1}, \quad t_1 \neq 0 \qquad [12]$$

is used to ensure that there is a nonzero population difference in these states after the conversion pulse. Our simulations show that pulse shaping has a similar effect on both pulses. Therefore, only the results relating to the second are shown here.

The simulations were carried out on an IBM RISC 6000 computer. The computing programs based on the above theoretical analysis were written in FORTRAN code. Because in our work the RIACT protocol was used the evolution time can be set to be larger than one spinning period, and full use of the periodicity of the Hamiltonian can be made to save CPU time and to avoid accumulated errors. The time step used in the computation depends on spinning speed as well as on the quadrupolar interaction parameters, the most important of which are the values of the QCCs and the asymmetry parameters. The partition of the solid angles (α, β) can be efficiently carried out by using the tetrahedron partitioning scheme of Alderman *et al.* (*47*). The simulations were performed for a spin-$\frac{3}{2}$ quadrupolar nuclear spin system with a variety of interaction parameters, spinning speeds, and RF fields. Shown below are some examples with a rotor spinning speed of 5 kHz and a maximum RF power of 60.0 kHz.

The conversion efficiencies with three different pulse shapes are shown in Fig. 1. As can be seen, for rectangular pulses, the sensitivity is uniform over a broad range of values. This means that it is unnecessary to set exactly the width of this pulse so long as it is in the uniform range. Whereas, when shaped pulses are used, the pulse duration must usually be set more carefully. As can be seen from the diagram, however, this requirement is not difficult to satisfy. The sensitivity can be maintained with shaped pulses. In Fig. 1, the same maximum RF power was used for all pulses; therefore, the total power applied to the probe is less when a shaped pulse is used.

Figure 2 gives a comparison of the intensity changes over a broad range of values of QCCs with three different pulse shapes, e.g., a rectangular pulse, a decaying triangular pulse,

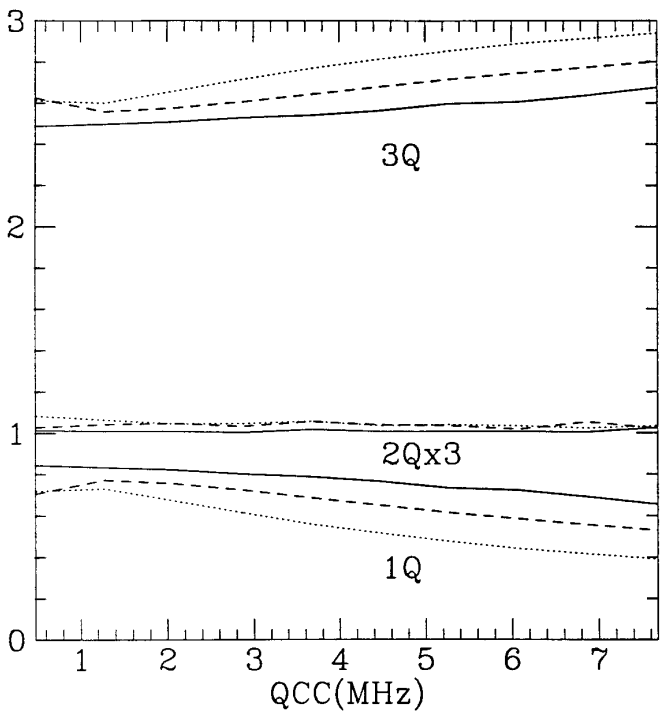

FIG. 2. The dependence of the conversion efficiency on the QCC values. The dashed lines are for a rectangular pulse (width $\frac{1}{4}\tau_r = 50.0$ μs), the dotted lines for a decaying triangular pulse (width $\frac{1}{4}\tau_r = 50.0$ μs), and the solid lines for the pulse defined by Eq. [10] (width $\frac{1}{4}\tau_r = 50.0$ μs). The parameters have the same values as those in Fig. 1 except $t_0 = \frac{1}{2}\tau_r = 100.0$ μs.

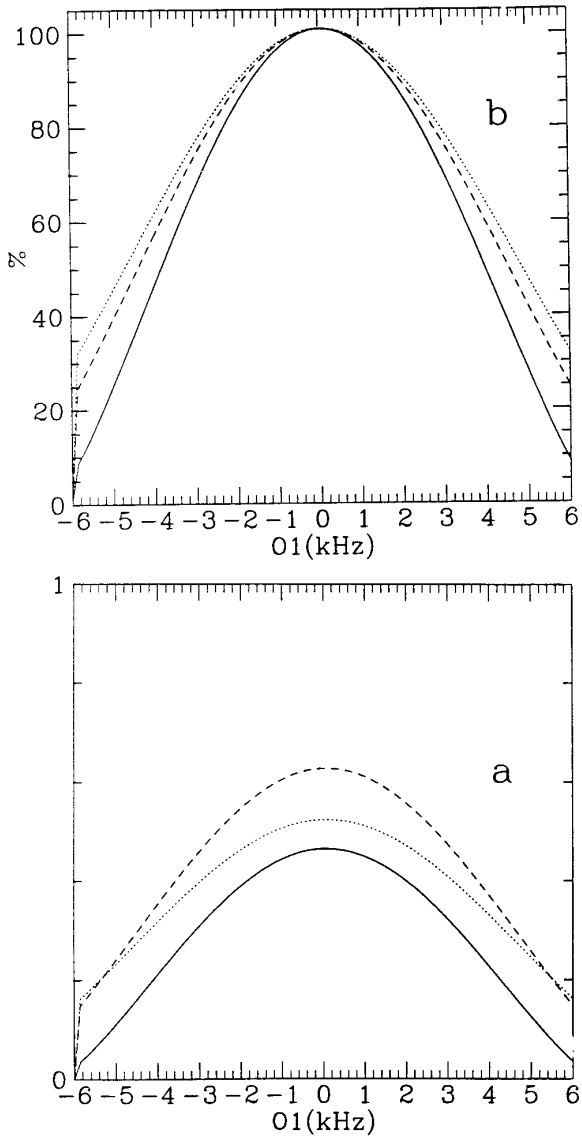

FIG. 3. The dependence of the 3Q conversion efficiency on RF offset, displayed with (a) the absolute intensities and (b) the (normalized) relative intensities. The dashed lines are for a rectangular pulse, the dotted lines for a decaying exponential pulse, and the solid lines for the pulse defined by Eq. [10]. The exponential pulse is defined as $\omega_1(t) = \omega_{1\max}e^{-bt}$, where $\omega_{1\max} =$ 60.0 kHz and $b = 6.0$ kHz. The other parameters have the same values as those in Fig. 1.

and the pulse defined by Eq. [10]. It is clear that the site quantification can be improved by optimizing the pulse shape. For example, a nearly horizontal line can be obtained by using the shape generated by Eq. [10].

Similar to Fig. 2, the intensity changes with different RF offsets for different pulse shapes are shown in Fig. 3. Figure 3a shows the variation of the absolute signal intensities (1QCs) with regard to offsets with three different pulse shapes: rectangular, decaying exponential, and the one defined by Eq. [10]. Figure 3b shows the change of relative intensities, i.e., the three intensities divided by their respective values at zero offset, which are a more accurate description of the offset tolerance. Note that the maximum RF power used is the same for all three pulse shapes. As can be seen from Fig. 3, the offset tolerance can be improved by properly adjusting the pulse shape; e.g., the decaying exponential shaped pulse is the best among the three used to yield the data for Fig. 3. It should be noted that the optimum shape with good offset tolerance might cause a reduction of sensitivity but the loss can be made quite small as shown in Fig. 3. Also, the best pulse shapes for quantification are not necessarily the optimum ones for improving offset characteristics.

Analogous results are obtained for the z-filtering case. Shown in Figs. 4–6 are the comparisons of conversion efficiencies of the three typical pulse shapes (for the second pulse), with different pulse lengths, QCCs, and RF offsets, respectively. It is obvious that the pulse shape (Eq. [10]) can significantly improve the site quantification problem caused by the large range of magnitudes of the QCCs although the offset effect is slightly degraded.

When higher RF fields or higher spinning speeds are used, the afore-mentioned results also hold but generally with higher sensitivity. It is noteworthy that in Figs. 1–3, although the spinning speed assumed is 5 kHz the sensitivity loss compared with higher spinning speeds is not drastic, meaning that shaped

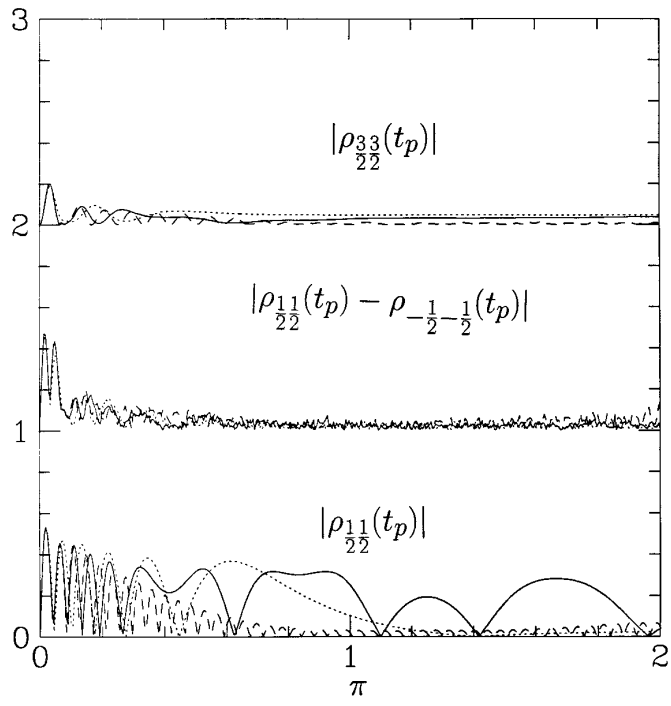

FIG. 4. The conversion efficiencies from the initial 3QC for different shaped pulses in the z-filtering case over a spinning period $[0,2\pi]$. The ordinates for $|\rho_{1/2,1/2} - \rho_{-1/2,-1/2}|$ and $|\rho_{3/2,3/2}|$ are shifted vertically by 1 and 2 units, respectively. The dashed lines are for a rectangular pulse, the dotted lines for a decaying triangular pulse, and the solid lines for the pulse defined by Eq. [10]. The parameters used are the same as those in Fig. 1.

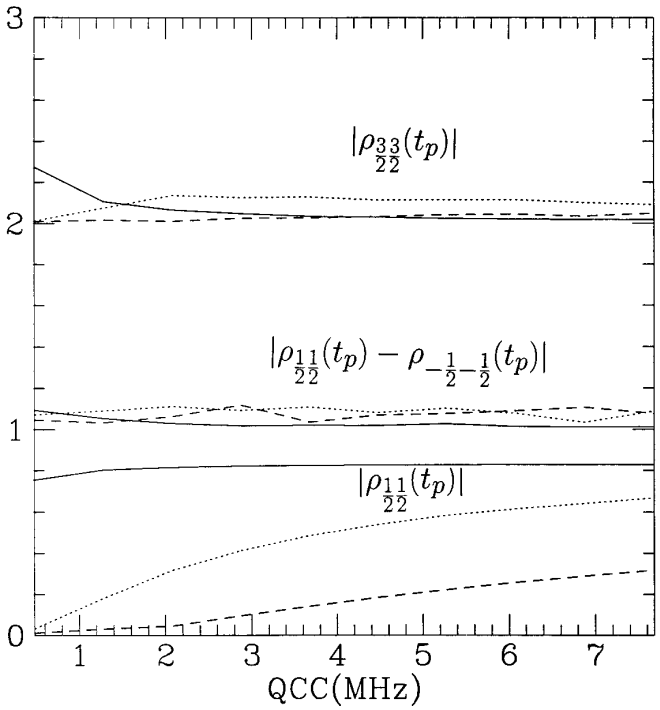

FIG. 5. The dependence of the 3Q conversion efficiencies on the QCC values in the *z*-filtering case. The ordinates for $|\rho_{1/2,1/2} - \rho_{-1/2,-1/2}|$ and $|\rho_{3/2,3/2}|$ are shifted vertically by 1 and 2, respectively. The dashed lines are for a rectangular pulse (width $\frac{1}{4}\tau_r = 100.0\ \mu s$), the dotted lines for a decaying triangular pulse (width $\frac{1}{4}\tau_r = 100.0\ \mu s$), and the solid lines for the pulse defined by Eq. [10] (width $\frac{1}{4}\tau_r = 50.0\ \mu s$). The other parameters have the same values as those in Fig. 2.

pulse MQMAS NMR can be performed with moderate spinning speeds. One problem related to slow or moderate spinning speeds is the occurrence of spinning sidebands in the isotropic dimension, meaning that the central band intensity is not a wholly reliable indication for use in site quantification analysis. However, for typical compounds, nuclei at all lattice sites may manifest spinning sidebands. Moreover, it is seen from Eqs. [5]–[9] that the pulse shaping has the same effect on the sidebands and the central band. Therefore, the relative increase of the central band intensity of certain sites corresponds to an improvement of the site quantification as compared with the original spectrum. On the other hand, there exist certain approaches that either restore the central band intensity and remove the spinning sidebands or reconstruct sideband-free spectra from the experimental ones combined with numerical fitting. This latter approach is under study.

3. EXPERIMENTAL RESULTS AND DISCUSSION

The experiments were performed on a Bruker MSL-200 NMR spectrometer. A Doty DAS probe was used with a spinning speed of about 6.5 kHz. The two-pulse sequence was used in our experiments. To compare the conversion pulse performance (quantification and offset effect), four types of second pulses were used: a short rectangular pulse as used in Refs. (1, 5–12), rectangular pulses with a duration of one-quarter of a spinning period as used in RIACT(I) (*39*), a decaying exponential pulse, and the shaped pulse defined by Eq. [10]. Pulse shaping can be easily realized on digital NMR spectrometers. In our experiments it was achieved with a homebuilt electronic circuit, a schematic diagram of which is shown in Fig. 7. The audiofrequency modulation signal is generated by an arbitrary wave generator. The modulation waveform (determined by the parameters including frequency, amplitude offset, and duration) is changeable by downloading different sets of data from a microcomputer connected to the waveform generator. The wave generator used was a Wavetek-75 with a maximum sampling frequency of 2 MHz; therefore, the time resolution in pulse shaping was 0.5 μs, sufficient for shaping pulses with a duration of approximately 100 μs as in our experiments. The modulation signal is then fed to a mixer circuit when a trigger signal (controlled by the pulse program) is applied to the wave generator. The mixed signal (shaped pulse) is first amplified by a low-power amplifier and later by a high-power amplifier. A variable attenuator can be used between the two amplifiers to adjust the output power. The linearity of the high-power amplifier is crucial for the production of an undistorted shape after amplifying. The amplifier attached to our MSL-200 was found to be nonlinear and thus unsuitable for our experiment. Therefore, a gateable linear high-power (ENI LPI-10, class-AB) amplifier was used.

The above theoretical predictions are verified by a series of experimental results for ^{23}Na 3Q–1Q MQMAS NMR correlation spectra from polycrystalline anhydrous Na_2HPO_4. There are three magnetically nonequivalent Na sites in this compound (*48*) with large QCC differences

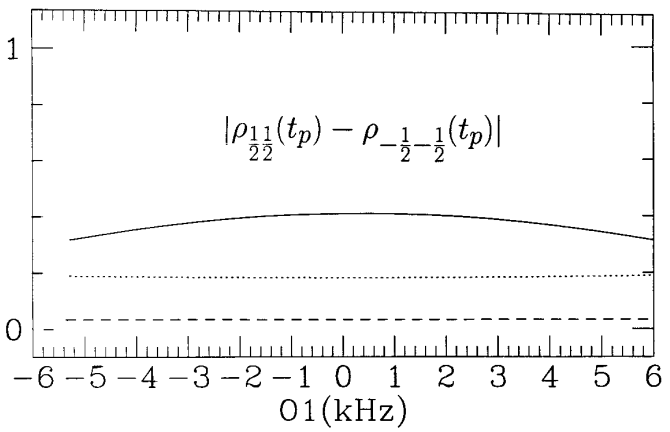

FIG. 6. The dependence of the 3Q conversion efficiency on RF offset in the *z*-filtering case, displayed with absolute intensities. The ordinate is the population difference of the two central energy levels, $|\rho_{1/2,1/2} - \rho_{-1/2,-1/2}|$. The dashed lines are for a rectangular pulse, the dotted lines for a decaying exponential pulse, and the solid lines for the pulse defined by Eq. [10]. The exponential pulse is defined as $\omega_1(t) = \omega_{1max}e^{-bt}$, where $\omega_{1max} = 60.0$ kHz and $b = 6.0$ kHz. The other parameters have the same values as those in Fig. 5.

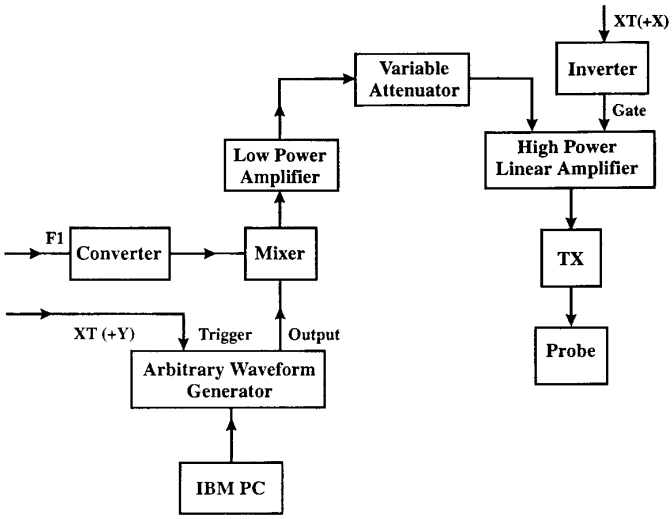

FIG. 7. The block diagram of the electronic circuitry used for high-power pulse shaping.

(2.13, 1.374, and 3.702 MHz); thus the undistorted isotropic solid-state NMR spectrum should show three peaks with a 1:1:2 intensity ratio (*48*). This compound has been generally regarded as an appropriate sample for testing the qualification by comparing the intensities of the three sites exhibited in its MQMAS spectrum. Demonstrated in Fig. 8 is the contrast between the spectra obtained with a short pulse, with the RIACT(I) scheme, and with the RIACT pulse sequence but employing a shaped pulse (Eq. [10]) for coherence conversion. It is clear that better site quantification is achieved by means of proper pulse shaping. For the spectrum generated with short pulses (Fig. 8a) (the normal MQMAS method), as expected, the intensity of the signal from site Na(3) is much weaker than the signals from the other two lattice sites, and, in addition, its linewidth is broader, meaning lower resolution. Even the intensities of the signals from the Na(1) and Na(2) lattice sites are not equal, though the two sites have relatively small and similar QCCs; this clearly means that other parameters such as the orientation of the EFG tensor of the quadrupolar nucleus at a particular site may also affect site quantification. As can be seen, the RIACT spectrum (Fig. 8b) exhibits little difference between the intensities of the signals from lattice sites Na(1) and Na(2), and there is also a significant enhancement of the intensity of the signal for lattice site Na(3). At higher magnetic fields and at higher spinning speeds, the RIACT method may offer better site quantification; see Ref. (*39*). As shown in Fig. 8c, site quantification is further improved in the MQMAS NMR spectrum obtained with the conversion shaped pulse defined by Eq. [10]. Considering that our experiment was performed on a relatively low-magnetic-field spectrometer with moderate rotor spinning speed, this enhancement of site quantification is meaningful and may be significant for future MQMAS NMR applications.

As pointed out in the previous section, one must note that under the above spinning speeds, the presence of spinning sidebands in the isotropic dimension may be significant; hence the central band intensity alone does not reflect quantitative information about the lattice site signal. A larger central band intensity, however, definitely corresponds to better quantification. A study is underway to devise a technique more general than the synchronized acquisition scheme (*15*) to remove the spinning sidebands and restore the intensity of the central band. If this technique proves practical, then the problem caused by insufficient spinning speed should become insignificant.

Figure 9 shows the contrast between the 3QC intensities in the MQMAS NMR spectra of Na_2HPO_4 obtained by using rectangular and decaying exponential pulses, and with various offsets. The normalized (Na(1)) integral intensities of the spectral peaks of the F1 projections are used. Obviously, with the decaying exponential pulse, better offset dependence can be achieved than with the rectangular pulse, in agreement with the theoretical results shown in Fig. 3. It is noteworthy that for different sites (with different QCCs), the offset curves are more similar to each other when a shaped pulse is used than when the

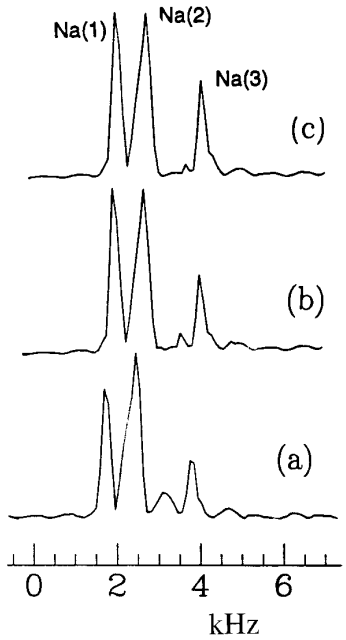

FIG. 8. Experimental ^{23}Na MQMAS NMR spectra of polycrystalline anhydrous Na_2HPO_4 acquired with (a) two short pulses (the second pulse length = 3 μs), (b) RIACT(I) with rectangular pulses (the second pulse length = 38.5 μs, one-quarter of the spinning period), and (c) the second pulse shaped (Eq. [10], with a pulse width of 115 μs, $a = 10\omega_1 = 700.0$ kHz, $b = 0.1\omega_1 = 7.0$ kHz, and $t_0 = 75.0$ μs). One hundred twenty-eight FIDs were acquired for each 2D spectrum with t_1 incremented in steps of 20 μs. One hundred twenty scans were used for each FID. The RF power was 70.0 kHz, the first pulse length = 12 μs, and the sample spinning speed was 6.5 kHz.

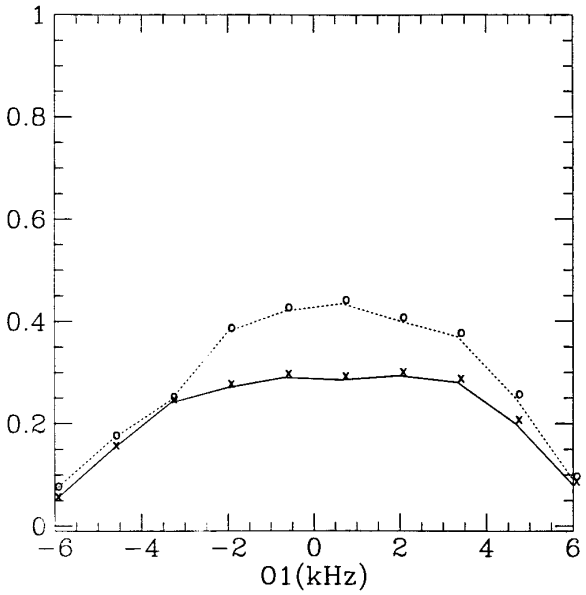

FIG. 9. The offset effect for the ^{23}Na MQMAS NMR spectra of polycrystalline anhydrous Na_2HPO_4 acquired with a rectangular pulse (circles) and a decaying exponential pulse $\omega_{1\max}e^{-bt}$ crosses. Integral intensities of the site Na(1) were used. The remaining sites (Na(2), Na(3)) have similar characteristics. For the case with shaped pulses, the pulse width was 115 μs, $\omega_{1\max}$ = 70.0 kHz, and b = 7.0 kHz. Other parameters were the same as those in Fig. 8c except for the change of the offset.

rectangular pulse is employed. This is understandable because the sensitivities with shaped pulses are much less dependent on the value of the QCC as shown in Fig. 2.

4. CONCLUSIONS

Through theoretical analysis supported by numerical simulations and experimental verification, a further perspective is presented on the effects of optimizing the MQMAS NMR pulse sequence, i.e., by means of pulse shaping. Two types of pulse shapes have been studied, namely, the sin x/x type and decaying exponential (or triangular) pulses. It is found that properly shaped pulses can enhance spectral site quantification and/or alleviate offset effects. This reduces the requirement of high rotor spinning speeds ($\geq$10 kHz) which is usually regarded as a prerequisite in MQMAS NMR spectroscopy. With the method described, MQMAS NMR studies may be carried out at moderate spinning speeds, thus becoming accessible to more experimenters. Moreover, the total RF power may be reduced to achieve the same sensitivity. Shaping can be carried out for the excitation, for conversion pulses, or for both. Although only spin-$\frac{3}{2}$ nuclear quadrupolar spin systems were considered in this work, the arguments supporting the use of shaped pulses are obviously applicable to higher spin cases and, therefore, similar results are expected for those systems. Finally, all the conclusions hold for the z-filtering case even though the optimum pulse length might be different. There may, of course, also exist more preferable pulse shapes that are more efficient than those presented here and they might be discovered, or designed, by using more powerful theoretical tools such as Floquet theory mentioned in Section 2. More work is being done along these lines and will be published separately.

ACKNOWLEDGMENTS

We are grateful to the Natural Sciences and Engineering Research Council of Canada for research grants to C.A.McD. We thank Thomas Marcus and Milan Coscizza for much helpful advice and significant technical assistance.

REFERENCES

1. L. Frydman and J. S. Harwood, *J. Am. Chem. Soc.* **117,** 5367 (1995).
2. A. Samoson, E. Lippmaa, and A. Pines, *Mol. Phys.* **65,** 1013 (1988).
3. A. Llor and J. Virlet, *Chem. Phys. Lett.* **152,** 248 (1988).
4. K. T. Mueller, B. Q. Sun, G. C. Chingas, J. W. Zwanziger, T. Terao, and A. Pines, *J. Magn. Reson.* **86,** 470 (1990).
5. A. Medek, J. S. Harwood, and L. Frydman, *J. Am. Chem. Soc.* **117,** 12779 (1995).
6. C. Fernandez and J. P. Amoureux, *Chem. Phys. Lett.* **242,** 449 (1995).
7. C. Fernandez and J. P. Amoureux, *J. Magn. Reson.* **5,** 315 (1996).
8. G. Wu, D. Rovnyak, B. Q. Sun, and R. G. Griffin, *Chem. Phys. Lett.* **249,** 210 (1996).
9. D. Massiot, B. Touzo, D. Trumeau, J. P. Coutures, J. Virlet, P. Florian, and P. J. Grandinetti, *Solid State NMR* **6,** 73 (1996).
10. J. P. Amoureux, C. Fernandez, and L. Frydman, *Chem. Phys. Lett.* **259,** 347 (1996).
11. C. Fernandez and J. P. Amoureux, *Chem. Phys. Lett.* **242,** 449 (1995).
12. J. P. Amoureux and C. Fernandez, *Solid State NMR* **10,** 211 (1998).
13. J. P. Amoureux, C. Fernandez, and S. Steuernagel, *J. Magn. Reson. A* **123,** 116 (1996).
14. S. P. Brown, S. J. Heyes, and S. Wimperis, *J. Magn. Reson. A* **119,** 280 (1996).
15. D. Massiot, *J. Magn. Reson. A* **122,** 240 (1996).
16. L. Marinelli and L. Frydman, *Chem. Phys. Lett.* **275,** 188 (1997).
17. J. P. Amoureux, D. P. Lang, M. Pruski, and C. Fernandez, *J. Magn. Reson.* **131,** 170 (1998).
18. R. E. Youngman, U. Werner-Zwanziger, and J. W. Zwanziger, *Z. Naturforsch. A* **51,** 321 (1996).
19. S. H. Wang, Z. Xu, J. H. Baltisberger, L. M. Bull, J. F. Stebbins, and A. Pines, *Solid State NMR* **8,** 1 (1997).
20. A. Samoson, *J. Magn. Reson. A* ***121,*** 209 (1996).
21. S. P. Brown and S. Wimperis, *J. Magn. Reson.* **124,** 279 (1997).
22. M. Pruski, D. P. Lang, C. Fernandez, and J. P. Amoureux, *Solid State NMR* **7,** 327 (1997).
23. C. Fernandez, L. Delevoye, J. P. Amoureux, D. P. Lang, and M. Pruski, *J. Am. Chem. Soc.* **119,** 6858 (1997).

24. S. H. Wang, S. M. De Paul, and L. M. Bull, *J. Magn. Reson.* **124,** 364 (1997).

25. J. V. Hanna, M. E. Smith, and H. J. Whitefield, *J. Am. Chem. Soc.* **118,** 5772 (1996).

26. J. H. Baltisberger, Z. Xu, J. F. Stebbins, S. H. Wang, and A. Pines, *J. Am. Chem. Soc.* **118,** 7209 (1996).

27. P. J. Dirken, S. C. Kohn, M. E. Smith, and E. R. H. van Eck, *Chem. Phys. Lett.* **266,** 568 (1996).

28. D. Massiot, R. Conanec, W. Feldmann, R. Marchand, and Y. Laurent, *Inorg. Chem.* **35,** 4957 (1996).

29. H. Kraus, R. Prins, and A. P. M. Kentgens, *J. Phys. Chem.* **100,** 16336 (1996).

30. C. Fernandez, J. P. Amoureux, L. Delmotte, and H. Kessler, *Microporous Materials* **6,** 125 (1996).

31. C. Fernandez, J. P. Amoureux, J. M. Chezeau, L. Delmotte, and H. Kessler, *Microporous Materials* **6,** 331 (1996).

32. J. Rocha, A. P. Esculas, C. Fernandez, and J. P. Amoureux, *J. Phys. Chem. 100,* 17889 (1996).

33. J. Rocha, Z. Lin, C. Fernandez, and J. P. Amoureux, *Chem. Commun.,* 251 (1996).

34. P. Sarv, C. Fernandez, J. P. Amoureux, and H. Kessler, *J. Phys. Chem.* **100,** 19223 (1996).

35. S. J. Hwang, C. Fernandez, J. P. Amoureux, J. Cho, S. W. Martin, and M. Pruski, *Solid State NMR* **8,** 109 (1997).

36. L. Delevoye, S. X. Liu, M. D. Welch, C. Fernandez, J. P. Amoureux, and J. Klinowski, *J. Chem. Soc., Farad. Trans.* **93,** 2591 (1997).

37. G. Wu, D. Rovnyak, P. C. Huang, and R. G. Griffin, *Chem. Phys. Lett.* **277,** 79 (1997).

38. G. Wu, S. Kroeker, R. E. Wasylishen, and R. G. Griffin, *J. Magn. Reson.* **124,** 237 (1997).

39. G. Wu, D. Rovnyak, and R. G. Griffin, *J. Am. Chem. Soc.* **118,** 9326 (1996).

40. S. Ding and C. A. McDowell, *Chem. Phys. Lett.* **270,** 81 (1997).

41. C. J. Lee, N. Murali, and W. S. Warren, *Adv. Magn. Reson.* **14,** 241 (1990).

42. J. H. Shirley, *Phys. Rev.* **138,** B979 (1965).

43. M. Maricq, *Phys. Rev. B* **25,** 66222 (1982).

44. Y. Zur, M. H. Levitt, and S. Vega, *J. Chem. Phys.* **78,** 5293 (1983).

45. T. Nakai and C. A. McDowell, *Mol. Phys.* **88,** 1263 (1996).

46. S. Ding and C. A. McDowell, *J. Chem. Phys.,* in press (1998).

47. D. W. Alderman, M. S. Solum, and D. M. Grant, *J. Chem. Phys.* **84,** 3717 (1986).

48. M. Baldus, B. H. Meier, R. R. Ernst, A. P. M. Kentgens, H. Meyer zu Altenschildesche, and R. Nesper, *J. Am. Chem. Soc.* **117,** 5141 (1995).